HiSST: 3rd International Conference on
High-Speed Vehicle Science Technology
14 -19 April 2024, Busan, Korea

A Study on the Aerodynamics and Aerothermodynamics of a Supersonic Reefed Parachute

Weijie Xu[1], Yi Li[2]

Abstract

Parachute, due to its low mass and high aerodynamic drag, is an important deceleration device in the fields of Earth's atmospheric re-entry deceleration, planetary entry, and deep space exploration. Supersonic parachutes, represented by disk-gap-band (DGB) parachutes, have gradually reached their maximum system mass and deployment velocity limits. To address this issue, researchers have designed a reefing system on the DGB parachute just like on the subsonic parachute, to reduce the inflation load to get a higher system mass and entry velocity. This paper establishes a reefed DGB parachute model based on the parachute of Mars Science Laboratory mission, and studies the aerodynamic and aerothermal characteristics of the supersonic reefed parachutes. Fluid-structure-interaction (FSI) technology is used to study the canopy inflation processes of reefed and disreefed parachute, and clarifies the aerodynamic characteristics such as drag and stability. Several typical states during the inflation process include mid-inflation state and canopy stable state are selected to establish corresponding parachute system models by computer-aided-design (CAD). The aerothermal characteristics of canopy macroscopic and microscopic structures are studied. Finally, the reefing design method suitable for the supersonic DGB parachute is obtained. All the works are to support deep space exploration such as Mars exploration.

Keywords: Reefed Parachute, Aerothermodynamics, Re-entry

Nomenclature

ASPIRE Advanced Supersonic Parachute Inflation Research Experiment

CAD computer-aided-design

CNSA China National Space Administration

DGB disk-gap-band

FSI fluid-structure-interaction

MSL Mars Science Laboratory

SHAPE supersonic high-altitude parachute experiment

1. Introduction

Parachute, as a typical aerodynamic deceleration device, has been widely used in aerospace engineering field due to its excellent low mass and high drag performance [1-4]. According to whether there are structural slots on the canopy, parachutes can be divided into solid textile canopies parachutes and slotted textile canopies parachutes. The solid textile canopy parachute with no structural slots on any part of the canopy except for the vent hole. This is the most basic form of parachute, such as flat circular canopy, extended skirt canopy, guide surface canopy, etc. (as shown in Fig. 1). The slotted textile canopy parachute is designed to improve the stability of the parachute and reduce the drag load during inflation with some structural slots on the canopy, such as cross canopy, ribbon canopy and DGB parachute (Fig. 2). For decades, supersonic parachute technology has developed rapidly to meet the needs of deep space exploration, planetary atmospheric re-entry, and high-altitude high-speed

[1] *Northwestern Polytechnical University, Youyi Xilu 127, xuweijie@mail.nwpu.edu.cn*
[2] *Northwestern Polytechnical University, Youyi Xilu 127, liyi_aerospace@foxmail.com*

deceleration. For example, due to the extremely thin atmosphere of Mars, its atmospheric density is only 1% of Earth's atmosphere [5]. In a series of Mars exploration missions by NASA and the CNSA (China National Space Administration), the DGB parachute has been used in all Mars landing missions. In the Mars Science Laboratory (MSL) mission, the parachute was deployed with an entry mass of 3257kg at Mach 2 [6]. In the Tianwen-1 mission of CNSA, the deployment speed was Mach 1.8 [7]. The system mass and velocity of probe have reached the performance limits.

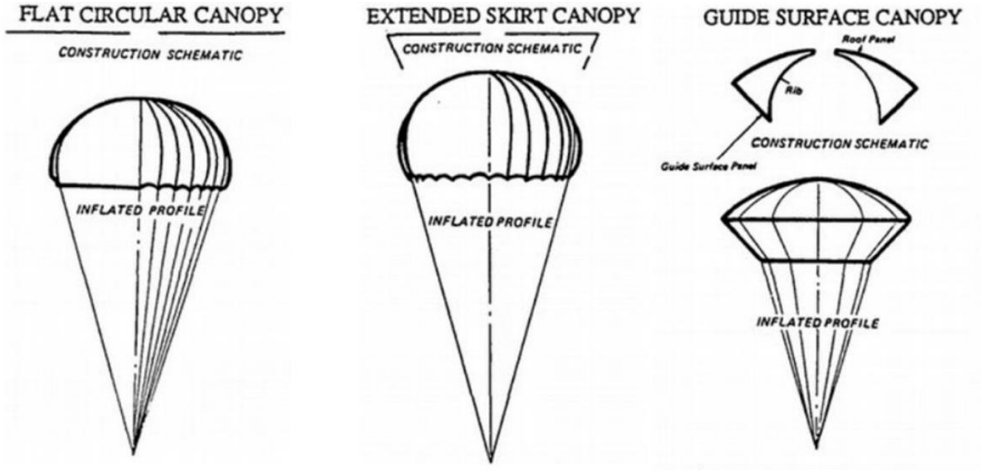

Fig. 1 Solid textile canopies, from the left side: flat circular canopy, extended skirt canopy, guide surface canopy [3]

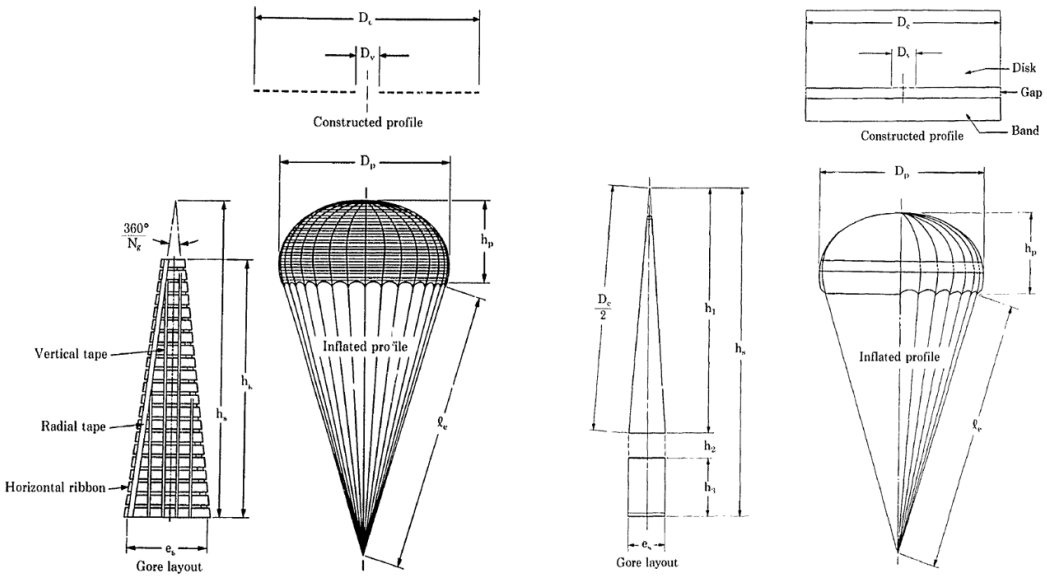

Fig. 2 Ribbon parachute (left) and DGB parachute (right) [4]

In order to reduce the drag load during parachute inflation, improve the probe mass and entry velocity, researchers have conducted a series of studies on the application of reefing systems on DGB parachutes. The reefing lines is a system of using limiting ropes or fabrics located in the middle, skirt region, vent hole, suspension lines, etc. of the parachute to gradually inflate the canopy. J. R. Schmidt [8] conducted flight experiments to study the relationship between the reefing ratio and the reefing area ratio of a quarter spherical ribbon parachute. The study showed that variations in canopy shape, nominal diameter, acid porosity cause little if any variation in the reefing curve. In Fallon's work [9], reefing line loads for Ares parachutes under a stable shape was studied. He got the relationship between drag load and axial force of the reefing lines. Christopher [10] calculated the steady-state canopy shape and flow field of a parachute under different reefing ratios based on experimental data of pressure distribution. In the 1970s, reefed and unreefed DGB parachutes with geometric permeability of 10%, 12.5%, and 15% were tested in low subsonic and supersonic wind tunnels to determine their stability and drag

performance [11], which proved the feasibility of the reefing system on parachutes with different geometric permeability. NASA [12] conducted high-altitude flight test of a DGB parachute using sounding rockets. The parachute was deployed at an altitude of 43.6 kilometers with a Mach number of 2.58. After a delay of 8.5 seconds, the parachute disreefed at Ma 0.99. This flight test showed that the installation of a reefed system effectively reduces the drag load during the inflation process, making the parachute system more stable. Witkowski and M. Kandis [13] conducted a series of mid-gore reefing tests using an MSL DGB parachute in a wind tunnel. The study showed that in the case of a mid-gore reefing, the parachute exhibits stable flight performance at all upstream speeds in the wind tunnel. During the NASA's supersonic high-altitude parachute experiment (SHAPE) program for Mars exploration [14], there were incidents of parachute damage and tearing. The final flight test summary analysis suggested that the thermal burning of the canopy material is caused by supersonic aerothermodynamics, and the annular burning area at the canopy is the theoretical stagnation point and surrounding area inside the canopy. After canopy inflation, the significant aerodynamic heat in the stagnation area inside the canopy leads to a sharp decrease of the load-bearing capacity of the canopy material, which induces the initial damage of the canopy and subsequent rapid expansion, tearing, and damage. Therefore, conducting aerodynamic and aerothermodynamics study of the inflation process of reefed supersonic DGB parachutes is important for the design of DGB parachutes.

This study aims to establish canopy models and microstructure canopy textiles models for reefed DGB parachutes in both reefed and fully inflated states, and conduct simulations to investigate the influence of aerothermodynamics on parachutes.

2. Method of simulation

2.1. Model to be simulated

This study establishes a 80-gore DGB parachute model with the reference of MSL parachute and Advanced Supersonic Parachute Inflation Research Experiment (ASPIRE) [15]. The structural parameters of parachute are shown in Table 1. The modeling method proposed by Daniel Z et al. in reference [16] is used to establish an initial pre inflation model for the parachute, as shown in Fig. 3 left. In FSI simulations, the disk and band of canopy are divided into 14000 elements using Belytschko-Tsay membrane model. The suspension lines are divided into 4080 elements using discrete beam model. The flow field is a cylindrical area with a diameter of 60m and a length of 150m, containing 2322000 elements.

Table 1 The structural parameters of parachute (unit: m)

Parachute ref diameter	Vent diameter	Disk diameter	Gap height	Band height	Suspension line length
21.55	1.52	15.64	0.9	2.6	36.52

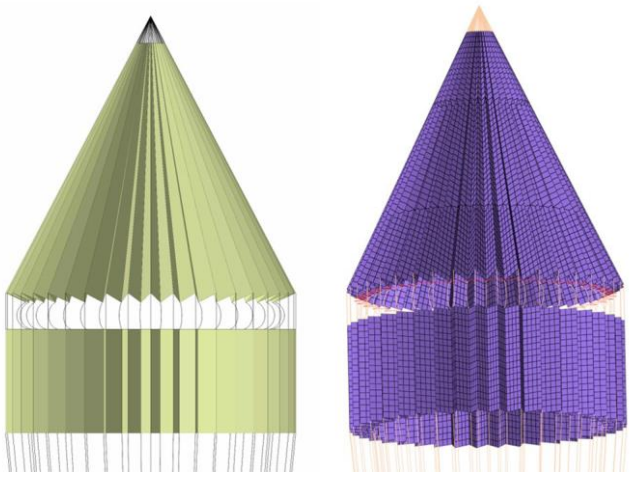

Fig. 3 Initial pre inflation model (left) and grid of canopy (right)

Angelova [17] approximated the woven structure to jet systems between fibers as circular and square holes in modeling the microstructure of canopy textiles. According to his research, the shape of the interstices can be either circular or square, as it does not practically affect the flow field after the woven structure. In this study, the pore structure between textiles is approximated as square. Considering the structure of fiber filaments, simplify the fiber cross-section into two types: square and circular, as Fig. 4 shows. The woven structure consisted of a brick of the size 0.213*1.098*1.098mm^3, immersed in a pipe-like domain, 4mm after the domain inlet and 8mm before the domain outlet, so that to assure the total flow formation.

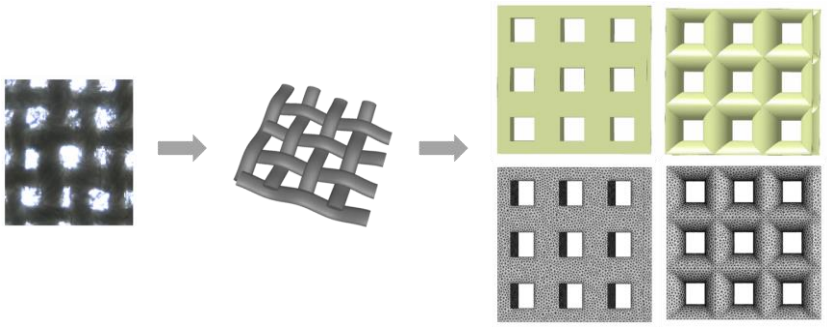

Fig. 4 Approximation of the woven structure to jet systems

2.2. Numerical method

Reynolds averaged Navier-Stokes (RANS) based mathematical model, implicit pressure based coupled solver and SIMPLE type algorithm are used in this study. Second order upwind discretization scheme was chosen together with Spalart-Allmaras (SA) one-equation turbulence model.

2.3. Validation of the numerical method

Based on the flight experimental conditions in ASPIRE SR03, the inflation process of a unreefed DGB parachute at Ma 1.88 is simulated to obtain drag load data. The simulation results and the flight test data in reference [15], the simulation data in reference [18] are shown in Fig. 5. In the verification simulation, the maximum parachute drag load is 308.9kN, with an error of 3.04% compared to the maximum drag load of 299.8kN in the flight test. At 0.3-0.8 seconds, due to the use of infinite mass models in the simulations of this study and Faisal's, the simulation results are in good agreement with Faisal's data, with an error of no more than 5%. There is a 15% error in the occurrence time of the maximum drag load in the simulation. Overall, in the design of supersonic parachutes, we are more concerned with the magnitude of the dynamic load, so the modeling and simulation methods in this study are feasible.

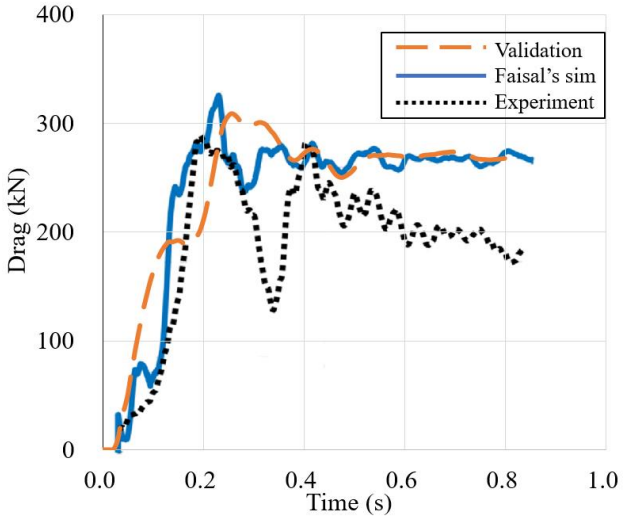

Fig. 5 Drag in kilo-Newton force as function of simulation time

3. Results and discussion

3.1. Inflation process of the parachute

In order to investigate the inflation process of a reefed parachute, a mid-gore reefing system is set for the established DGB parachute earlier. The length of reefing line is 33.85 meters, with the reefing ratio of 0.5. The initial simulation speed is Ma 1.88, when the parachute is straightened. Fig. 6 shows the inflation process of the reefed parachute. As the canopy inflates, a low-speed and high-pressure area gradually forms inside the canopy, and a detached shock wave is formed in the front of the skirt region. There is a periodic canopy breathing phenomenon after 0.38 seconds. After a period of delay, the parachute disreefed at Ma 0.8. The canopy continues to inflate until fully inflated. The parachute exhibits stability throughout the deceleration process. The reefed system effectively reduces the inflation drag of the supersonic DGB parachute.

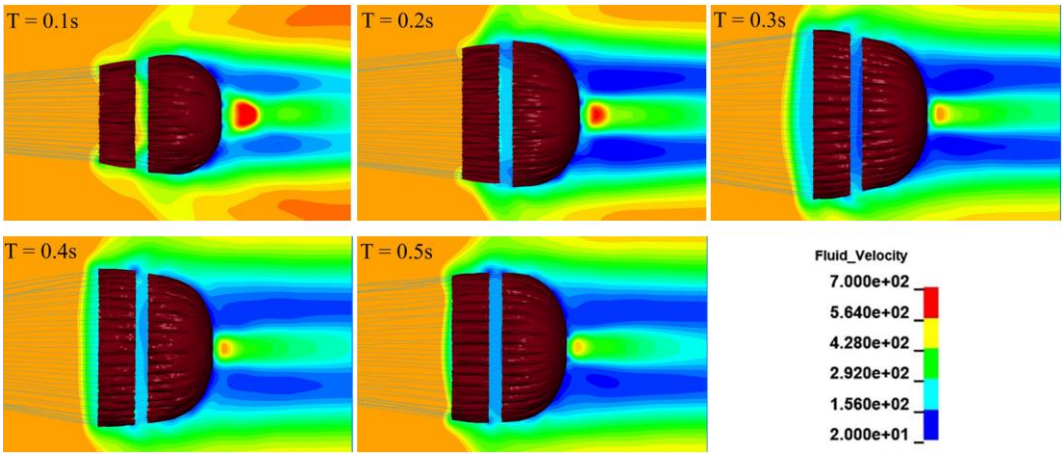

Fig. 6 Inflation process of the reefed parachute

In order to further investigate in detail the aerodynamic and aerothermodynamics characteristics of parachute canopy in semi inflated and fully inflated states, two stable states (reefed canopy of 0.5s and disreefed canopy of 0.8s) are selected to establish the canopy model as shown in Fig. 7. The suspension lines and reefing line are ignored when modelling. For the convenience of modelling and CFD simulation, the thickness of the canopy model has been expanded to 100mm. Perform CFD simulations on them to obtain the relevant parameters of the point with the maximum heat flux and the point with the maximum pressure differential between the inner and outer surfaces of the canopy. Use these parameters as input conditions for the simulation of microstructure canopy textile. The atmospheric model of all the simulation refers to the ASPIRE SR03 flight test.

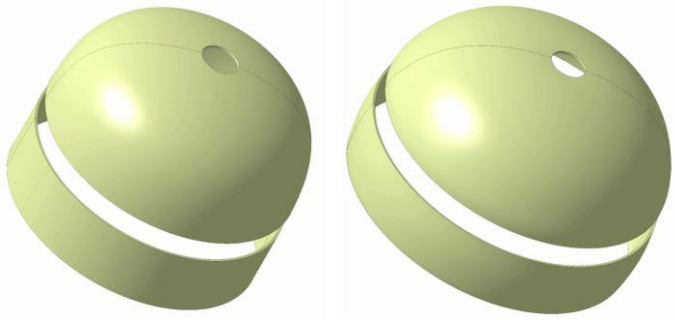

Fig. 7 Reefed (left) and disreefed (right) canopy model

Fig. 8 and Fig. 9 show the CFD simulation results of the canopy under different states and velocities. The maximum heat flux of the supersonic reefed canopy is 4769.48W/m^2, and the maximum heat flux of the subsonic disreefed canopy is 2296.68W/m^2. The geometric shape and velocity of the canopy are different, and the maximum heat flux on the surface of the canopy differs by more than twice, but both have similar flow characteristics. The maximum heat flux points for both supersonic and subsonic canopies are at the edge of the canopy, such as the leading edge of the disk and the edge of the vent

hole (left side of Fig. 8 and Fig. 9). Throughout the entire deceleration process, the edge of the parachute is always the most adverse part of thermal environment. When designing a parachute, edge stiffener is placed at the edges of the canopy to ensure structural strength and prevent tearing. This design also avoids the structural strength reduction caused by aerodynamic heating of the parachute. The pressure distribution on the inner and outer surfaces of the canopy is shown on the right side of Fig. 8 and Fig. 9. The stagnation point and surrounding area of the canopy are the area where the maximum pressure differential between the inside and outside of the canopy. That becomes the most significant area in terms of its permeability characteristics. In reference [14], the parachute was damaged during flight tests, and the theoretical analysis of the cause of the damage is similar to the simulation results in this paper. The area near the stagnation point may become the harshest thermal environment in the actual operation of parachute. To further investigate the impact of different pressure differentials on the aerodynamic performance of parachute textiles, four sets of pressure data (the maximum heat flux point and maximum pressure differential point of the canopy in the reefed and disreefed states) are selected as characteristic data. Simulations are conducted on the circular and square textile cross-section models. The data list is shown in Table 2.

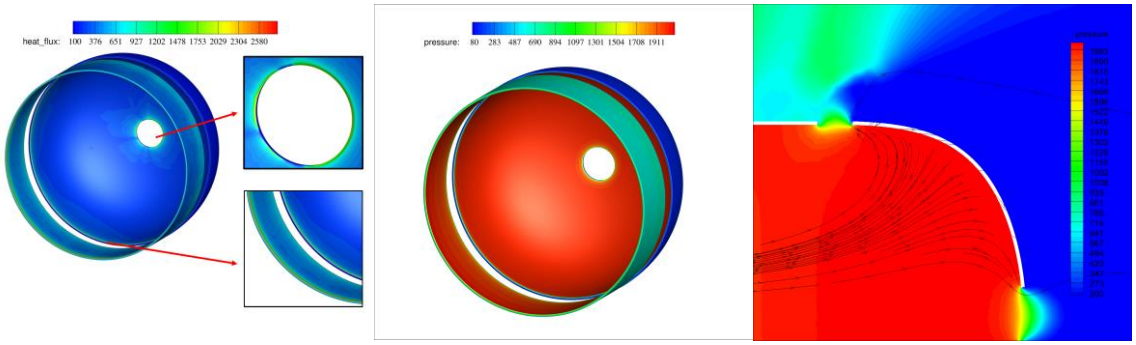

Fig. 8 Heat flux (left) and pressure contour (right) of reefed canopy

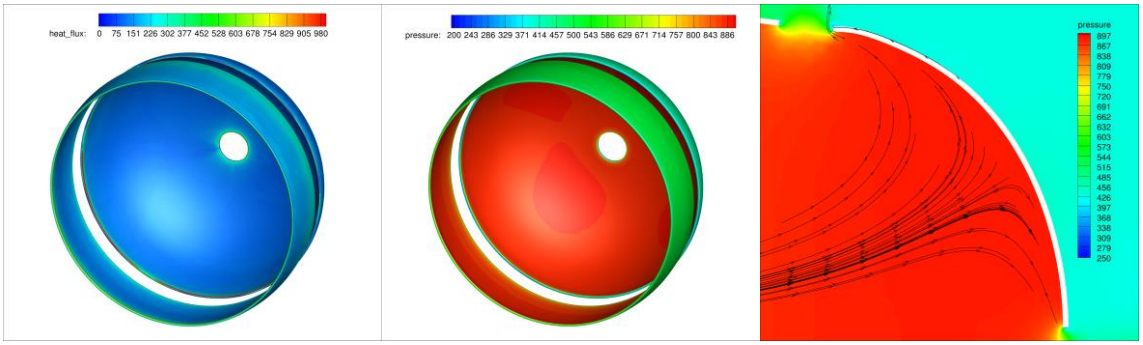

Fig. 9 Heat flux (left) and pressure contour (right) of disreefed canopy

Table 2 Data list of feature points

No.	model	Case	Inner surface pressure (Pa)	Outer surface pressure (Pa)
1	Reefed	Maximum heat flux	2114.68	135
2		Maximum pressure differential	1728.955	650
3	Disreefed	Maximum heat flux	915.832	435.975
4		Maximum pressure differential	666.365	424.144

3.2. Aerodynamic characteristics of canopy textile with different pressure differentials

Fig. 10 and Fig. 11 show the pressure and velocity contour of circular and square fiber models under four different cases. The three pores on the same cross-section in the figure exhibit the same flow characteristics, proving the rationality of using a 3*3 pore structure for modeling. This modeling method has been validated in Angelova's research [17]. When the pressure on both sides of the fabric is different, there is a significant difference in the flow velocity through the fabric holes. When the pressure

ratio of both sides of the fabric is less than the critical pressure ratio, the flow at the throat or pore outlet position is acoustic flow. It should be noted that B.A. Shannak's research indicates that for orifice flow, the critical pressure ratio is much smaller than the value obtained from the assumption of isentropic flow [19]. The velocity contours exhibit similar structures in the simulations of circular and square fiber models. When the pressure ratio of both sides of the parachute is lower than the critical pressure ratio, the flow through the parachute canopy fabric pores is similar to the flow through the rocket engine nozzle. The flow velocity at the minimum aperture reaches the speed of sound (represented by the throat in the circular model and the outlet position in the square model) and continues to increase downstream. When the pressure ratio is higher than critical pressure ratio, the flow velocity remains below the speed of sound and begins to slow down in the latter half of the pores. At this point, the maximum velocity position moves forward, and the wake attenuation zone significantly shortens. The length of the wake region varies with changes in pressure differential and pressure ratio. But the change in pressure is exactly the opposite, with pressure decreasing along the direction of flow. The pressure change is mainly manifested in the pores of the canopy fabric, and the pressure gradient value in the canopy fabric area is much greater than that in the upstream and downstream areas of the canopy. In all cases, the pressure will rapidly decrease upon reaching the pore position and decrease to near the back pressure of the canopy or slightly below the back pressure. The length of the high-pressure gradient region is independent of the pressure differential and pressure ratio, and does not exceed 1.5 times the thickness of the canopy. In addition, due to the different wall structures of the model, vortices are more likely to occur on the leeward side of the square fiber model.

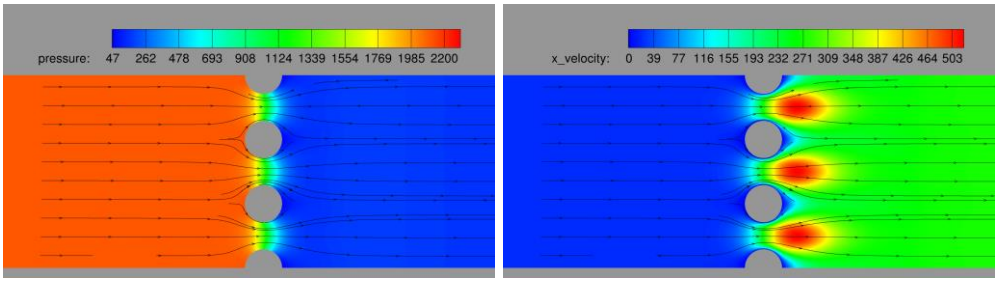

(a) case 1 with circular fiber model

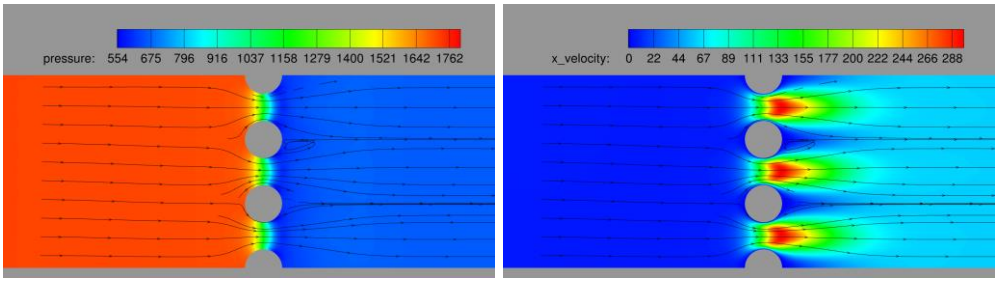

(b) case 2 with circular fiber model

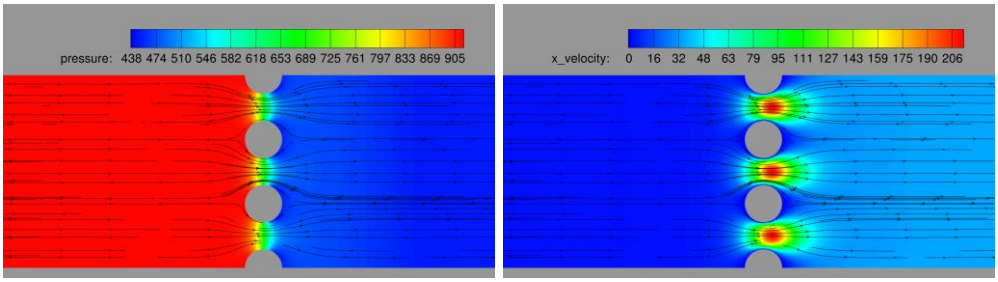

(c) case 3 with circular fiber model

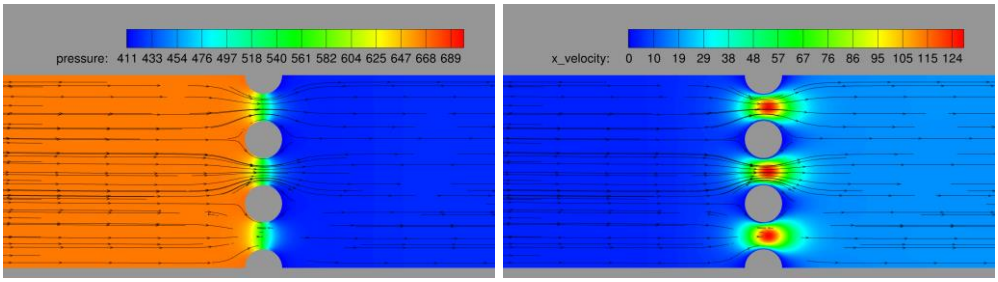

(d) case 4 with circular fiber model

Fig. 10 Pressure (lift) and x_velocity (right) contour of circular fiber model

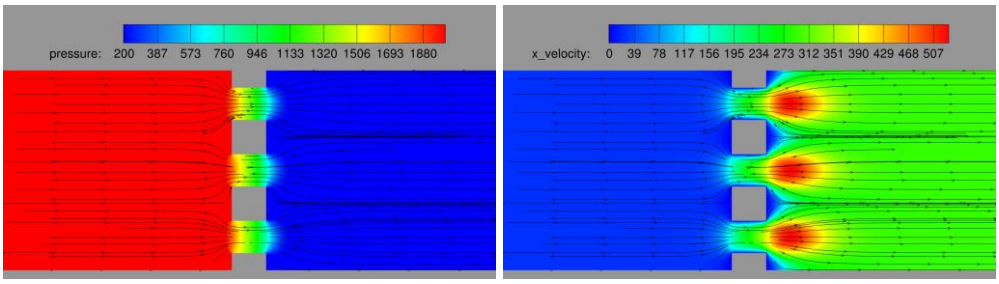

(a) case 1 with square fiber model

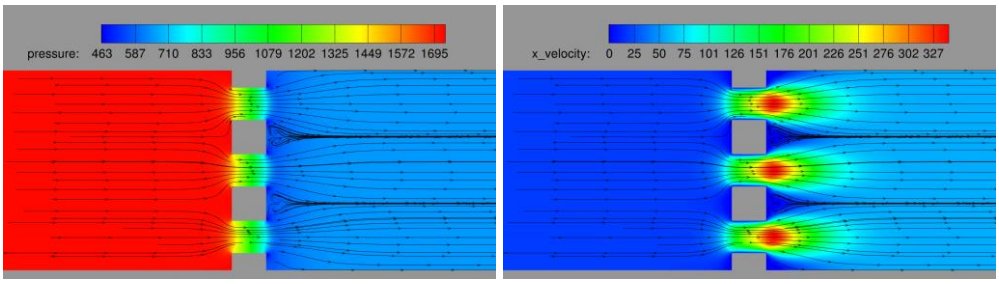

(b) case 2 with square fiber model

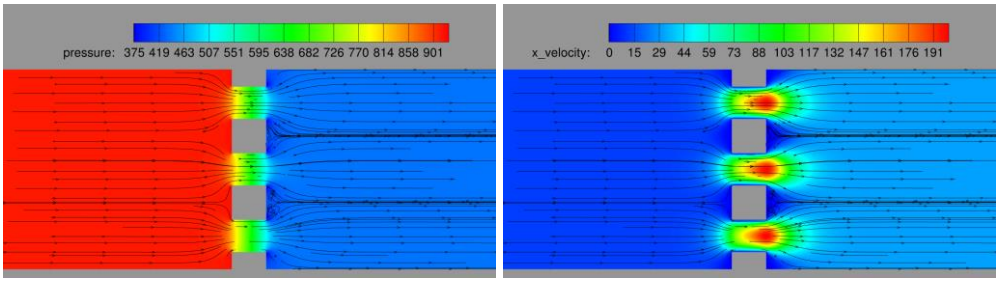

(c) case 3 with square fiber model

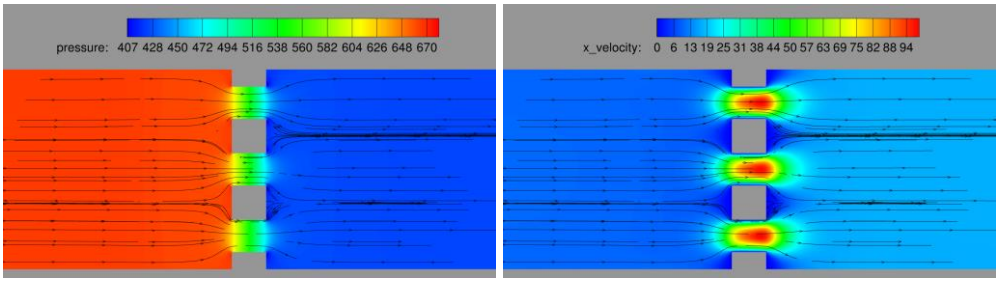

(d) case 4 with square fiber model

Fig. 11 Pressure (lift) and x_velocity (right) contour of square fiber model

4. Conclusions

In this work, the numerical simulations are carried out to investigate the inflation behaviors of a reefed DGB parachute, and conduct aerothermodynamics research on the macro canopy structure and micro fabric structure:

a) The supersonic DGB parachute exhibits a strong breathing phenomenon when reefed.

b) The maximum heat flux points of a DGB parachute occur at the edge of the canopy, including the leading edge of the disc and band, and the edge of the vent hole.

c) The stagnation point and attachment area inside the canopy are the areas with the highest pressure differential, and the canopy penetration characteristics are the most significant.

d) The pore flow characteristics of parachute canopy are similar to those of rocket engine nozzles. Under high altitude and high speed conditions, the pressure ratio of inner and outer surfaces of canopy is smaller. The flow at the pores of the canopy is more prone to supersonic flow.

e) The length of fabric pore wake zone varies with the variation of pressure differential and pressure ratio.

f) The circular and square fiber cross-section models have similarities in pressure and velocity distribution. Except for the vortex distribution on the leeward side of the fiber, the model has little effect on the flow.

References

1. Xiaopeng Xue, Chih-Yung Wen, Review of unsteady aerodynamics of supersonic parachutes, Progress in Aerospace Sciences, Volume 125, 2021, 100728.

2. J.R. Cruz, J.S. Lingard, Aerodynamic decelerators for planetary exploration: past, present, and future, AIAA Paper 2006-6792, 2006.

3. D.J. Cockrell, The Aerodynamics of Parachute, AGARD-AG-295, 1987.

4. R.C. Maydew, C.W. Peterson, Design and Testing of High-Performance Parachutes, AGARD-AG-319, 1991.

5. Jush H L. Justus C G. Mars global reference atmospheric model (Mars-GRAM 2005) applications for Mars science laboratory mission site selection process[C].Seventh International Conference on Mars. Pasadena,California.2007.

6. P. Subrahmanyam, D. Rasky, Entry, Descent, and Landing technological barriers and crewed MARS vehicle performance analysis, Prog. Aero. Sci. 91 (2017) 1–26.

7. Rao W, Sun Z Z, Dong J, et al. Design and implementation of the Mars entry, descent, and landing system for the Tianwen-1 mission , J. SciSin Tech, 2022, 52: 1162–1174.

8. J.R. Schmidt, P.G. McFadden, Reefing of Quarter Spherical Ribbon Parachutes Used in the Ares I First Stage Deceleration System, 20th AIAA Aerodynamic Decelerator Systems Technology Conference and Seminar Aerodynamic Decelerator Systems Technology Conferences, Washington, 2009, 4-7 May.

9. Dean Wolf, E.J. Fallon, Reefing Line Loads for Ares Parachutes, 21st AIAA Aerodynamic Decelerator Systems Technology Conference and Seminar, Dublin, 2011, 23-26 May.

10. Christopher, Jason Daniel, Computational aerodynamics modeling of the reefed stages of ringsail parachutes, Houston, Rice University, 2009.

11. Mayhue, R. J. et al. Supersonic and subsonic wind-tunnel tests of reefed and unreefed disk-gap-band parachutes. 1970.

12. J.S. Preisser and R.B. Grow, High-Altitude Flight Test of a Reefed 12.2-Meter-Diameter Disk-Gap-Band Parachute with Deployment at a Mach Number of 2.58, NASA TND-6469, 1971.

13. A. Witkowski, M. Kandis, Reefing the Mars Science Laboratory parachute, 2010 IEEE Aerospace Conference, Big Sky, MT, USA, 2010.

14. Eckstrom, Clinton V.: Flight Test of a 40-Foot-Nominal-Diameter Disk-Gap-Band Parachute Deployed at a Mach Number of 3.31 and a Dynamic Pressure of 10.6 Pounds Per Square Foot. NASA TM X-1924, 1970.

15. C. O'Farrell, B. S. Sonneveldt, C. Karhgaard, J. A. Tynis and I. G. Clark, Overview of the ASPIRE Project's Supersonic Flight Tests of a Strengthened DGB Parachute, 2019 IEEE Aerospace Conference, Big Sky, MT, USA, 2019.

16. Daniel Z. Huang, Philip Avery, Charbel Farhat, Jason Rabinovitch, Armen Derkevorkian and Lee D. Peterson. Modeling, Simulation and Validation of Supersonic Parachute Inflation Dynamics during Mars Landing, AIAA 2020-0313. AIAA Scitech 2020 Forum. January 2020.

17. Angelova, R.A., Stankov, P., Simova, I. et al. Three dimensional simulation of air permeability of single layer woven structures. cent.eur.j.eng 1, 430–435 (2011).

18. F. As'ad, P. Avery, C. Farhat, J. Rabinovitch, M. A. Lobbia, Validation of a high-fidelity supersonic parachute inflation dynamics model and best practice, AIAA SCITECH 2022 Forum (2022).

19. B.A. Shannak. Experimental Investigation of Critical Pressure Ratio in Orifices[J]. Experiments in Fluids, 33 (2002) 508–511. DOI 10.1007/s00348-002-0438-3.